Springer

KSME

Journal of Mechanical Science and Technology 29 (6) (2015) 2535~2545
www.springerlink.com/content/1738-494x(Print)/1976-3824(Online)
DOI 10.1007/s12206-015-0545-8

Influence of combined radial location and growth on the leakage performance of a rotating labyrinth gas turbine seal †

Sivakumar Subramanian[1], A. S. Sekhar[1,*] and B. V. S. S. S. Prasad[2]

[1]*Machine Design Section, Department of Mechanical Engineering, Indian Institute of Technology Madras, Chennai, 600036, India*
[2]*Thermal Turbomachines Laboratory, Department of Mechanical Engineering, Indian Institute of Technology Madras, Chennai, 600036, India*

(Manuscript Received June 12, 2014; Revised December 25, 2014; Accepted February 3, 2015)

Abstract

Leakage characteristics, influenced by centrifugal and thermal radial growth are determined computationally for a generic rotating labyrinth seal used in the gas turbine secondary air system. Three seal locations, namely, R25, R50 and R75 are represented by means of varying the rotor radius mimicking different radial positions of the seal from the shaft axis. The combined influence of seal location and its radial (Centrifugal and thermal) growth on the leakage performance is investigated for a wide-ranging speeds from 1000 to 3000 rad/s, temperatures ranging from 200 to 450 ^{o}C and pressure ratios varying from 1.1 to 2.5, for a chosen initial clearance of 500 micron. A comparison of the effect of rotation and temperature gradient among different rotors shows that the radial growth and leakage flow rates significantly vary with the increasing radius.

Keywords: Centrifugal/thermal/radial growth; CFD/FEA; Gas turbine; Leakage performance; Radial location; Rotating labyrinth seal

1. Introduction

Labyrinth seals are principal components used in a gas turbine (GT) secondary air system for reducing the air leakages and directing the air to cool certain critical components. When the engine is under operation, the seals are subjected to high rotational speed (Mechanical load) as well as elevated temperature (Thermal load). They are prone to experience both centrifugal and thermal deformations predominantly in the radial direction. Consequently, the radial clearance of the seals, under operation, varies from the initial clearance. Further, as these seals are placed at different radial locations, they experience distinctly different radial growth and hence varied leakage performance. Thus, the accurate knowledge of the radial growth at different locations and the subsequent influence on leakage aids in deciding their initial clearance.

There are a few critical reviews available in the Refs. [1-5], pertaining to plain annular seals, labyrinth seals, brush seals and advanced seals used in gas turbine secondary air systems. The work by Wittig et al. [6] contained static rig experiments as well as numerical investigations for geometrically similar straight through and stepped seals of converged and diverged configurations. They reported the values of coefficient of discharge for various clearance sizes for stepped and straight through seals. Childs and Vance [7] suggested the choice of different class of seals including labyrinth, plain annular, honey comb and pocket damper stator seals for various applications and reported results from analyses and tests. They also presented the traditional rotordynamic model used for predicting the reaction force components of an annular gas seal. Prasad et al. [8-10] had performed both experimental and numerical investigations of different labyrinth configurations, namely, straight-through, inclined and radial labyrinth seals. Kim and Cha [11] presented a comparative analysis of the influence of configuration and clearance on the leakage behavior of labyrinth seals using CFD and reported leakage flow pattern for various clearances. However, all the studies reported earlier had confined their investigations to static cold conditions, thus neglected rotation and thermal effects.

The limitations of the static rig and the need for rotating test rig were recognized later when Proctor and Delgado [12, 13] had carried out seal leakage tests in the "NASA high speed, high temperature turbine seal test rig". They tested various seals in this rig, from a classical labyrinth seal to an advanced finger seal, with operating conditions up to 650 °C of air temperature, 5.17 bar pressure, and linear speeds up to 366 m/s. Further work by Paolillo et al. [14, 15] and Zhigang Li et al. [16] have augmented this understanding when they developed their rotating rigs to test labyrinth [14], stepped [15] and staggered labyrinth [16] seals. In recent years, the need for the consideration of centrifugal and thermal growth is recognized.

*Corresponding author. Tel.: +91 44 2257 4709(0), Fax.: +91 44 2257 4652
E-mail address: as_sekhar@iitm.ac.in
† Recommended by Associate Editor Tong Seop Kim

Gamal et al. [17] accounted for the centrifugal growth of plain solid shaft using an empirical formula while testing a pocket damper seals (PDS). However, they maintained the teeth as principally static. Zhigang Li et al. [18] estimated the centrifugal growth using a FE model for the prediction of leakage flow of PDS. They compared their FEA results with the Roark's formula [17] and reported that analytical estimations are higher than those of the FEA results. Further, in both Refs. [17, 18], the thermal growth is ignored, possibly because their tests are carried out at 10 to 17 ^{o}C. Li et al. [19] estimated the centrifugal growth using a FE model for the prediction of leakage flow of a labyrinth brush seal. They too neglected the thermal growth. Some of the recent works [20, 21] took into account the stator/rotor deflection pertaining to a particular flight cycle; but quantification of centrifugal and thermal growths and their influence on air leakage were not presented.

Thus, systematic investigations presenting the effect of both centrifugal and thermal growth on the leakage characteristics of rotating gas turbine seals are seldom reported. Taking cognizance of this fact, present authors accounted for both centrifugal and thermal growth to predict the operating clearance and to estimate leakage flow rate in a six-tooth straight-through rotating labyrinth seal. A model developed by the authors [22, 23], based on combined computational fluid dynamics (CFD) and finite element (FE) methodology, is shown in Fig. 1. In these papers, the CFD methodology is numerically validated against the results reported by Kim and Cha [11]. The growth values predicted with different boundary conditions, by FEA, are compared against an analytical model and are found to agree closely when the fix-free end conditions are applied [22]. The present study focuses on fix-free edge conditions of the seal, which is more common in a typical aero-engine. Thus, the present paper is a continued computational attempt to gain insight into the influence of (i) radial growth (Determined with fix-free edge conditions) of the seal and (ii) seal location, on its leakage performance. The same seal configuration used by the authors of Refs. [6, 11] is used in this work as well.

2. Methodology

Table 1 provides the geometric details of the rotating labyrinth GT seal configuration, at three different locations, namely, R25 (Small rotor), R50 (Medium rotor) and R75 (Large rotor). These locations are represented by varying the shaft radius and mimicking different radial positions of the seal from the shaft axis. The seal configuration is shown in Fig. 2, which is similar to that of used in the earlier studies [6, 11]. The principal reason for choice of this profile is to validate the base model with the available numerical and experimental data in the literature. Although the profile is a simple one, it is generic in nature. The methods used in the investigation are also relevant and applicable to more advanced seals used in the gas turbine secondary air systems. The reduced operating clearance owing to the centrifugal growth alone and the net reduced operating clearances due to the combined centrifugal and thermal growth are calculated based on the radial growth of seal obtained from FEA. Although both the rotor and stator experience thermal growth in a real engine, the stator deformations are presumed to be negligible and not accounted in the present study.

Table 1. Geometrical details of seal.

Seal parameter	L	R	C	p	b	h
Values (mm)	86.5	25-75	0.5	12	2.5	10.5

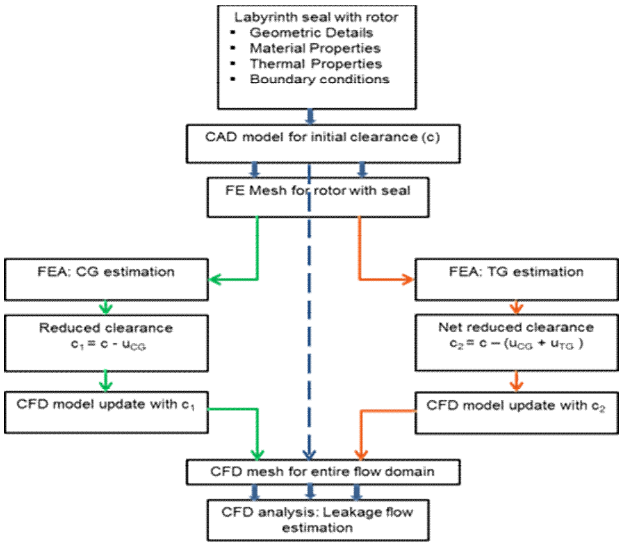

Fig. 1. Block diagram for labyrinth seal clearance model [22].

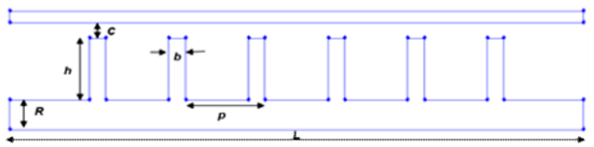

Fig. 2. Labyrinth GT seal configuration (not to scale).

2.1 CFD model

The computational flow domain essentially comprises of inlet, outlet, rotor wall and stator wall. One of the main reasons for selecting such an extended inlet and outlet is to ensure that the boundary conditions do not have an undesirable effect on the leakage flow through the seal. Fig. 3 depicts the typical computational domain for R75. A 3D multi-block structural grid is created in ANSYS ICEM CFD 14. The fluid is air; the flow is considered as steady, compressible and turbulent. The initial air temperature is taken as 300 K. The absolute pressure values are prescribed at both inlet and outlet. Atmospheric pressure is maintained at the outlet. Thus, the inlet pressure is calculated from pressure ratio which is defined as the ratio of absolute pressure at inlet and outlet. Three-dimensional Rey-

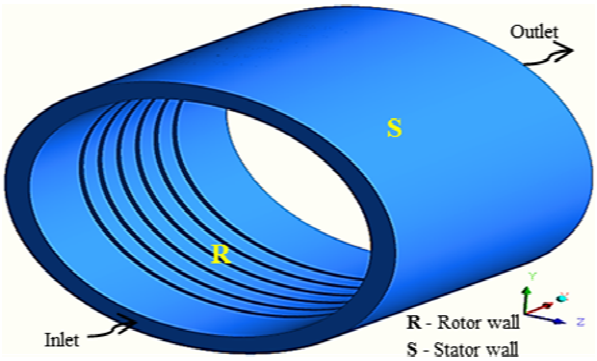

Fig. 3. Flow domain for R75 with initial clearance 0.5 mm.

nolds Averaged Navier-Stokes compressible equations are solved together with the additional transport equations for the turbulent kinetic energy and the turbulent dissipation rate. A standard k-ε model, with enhanced wall treatment, available in ANSYS FLUENT 14, has been incorporated into the analysis. The detailed description of this problem and its numerical treatment were clearly discussed in the previous work [22]. Although the present problem is amenable for an axisymmetric analysis, a full 3-D model (360°) has been used. The CFD model is validated by comparing with (i) the earlier numerical result of Kim and Cha [11] in Figs. 4(a) and (ii) the experimental result of Wittig et al. [6] in Fig. 4(b) for the same conditions. It is inferred from Fig. 4 that the present 3D model differs by about 6% compared to 2D CFD model [11], but is closer to the test data [6].

A detailed grid sensitivity analysis, similar to that of reported in Hirano et al. [24] is carried out to ensure the spatial accuracy of the solver. Accordingly, the number of divisions along the longitudinal and circumferential direction is arrived first followed by the lateral direction. Then the nodes in the clearance gap are varied. More nodes are clustered near the walls to account for a possible change of flow. This is achieved by employing appropriate mesh law "Bi-geometric" code available in ANSYS ICEM CFD 14. Typical results for R75 configuration at an angular speed of 1000 rad/s and pressure ratio of 1.9 is shown in Fig. 5. The numbers 10, 15, 20, 25, 30, 40 denote the number of radial nodes in the clearance and it can be inferred that the increase in grid size from 2887200 to 4101600 nodes exhibits an insignificant change. Thus, the present mesh with 20 nodes in the clearance region is found adequate to predict the leakage flow rate. Furthermore, the grid adequacy is ensured by calculating the fine grid convergence index (GCI), which is found to be less than 1%. Similar studies have been carried out for R25 and R50 to ensure the accuracy of the solver. Consequently, the grid size of about 0.9, 1.9 and 2.9 million nodes has been chosen for R25, R50 and R75, respectively.

Fig. 6 shows the typical CFD grid generated for R75 configuration. The details of the grid used for the various cases investigated are furnished in Table 2. It may be noted that the

Table 2. CFD grid details for various cases.

Seal region	Number of nodes for various cases
Circumference	80 (R25), 160 (R50), 240 (R75)
Inlet to tooth 1 (Axial)	40
Tooth 6 to outlet (Axial)	40
Cavity width (Axial)	25
Tooth width (Axial)	10
Tooth height (Radial)	35
Clearance gap (Radial)*	20^1,15^2,10^3

*Superscript 1 denotes for initial and reduced clearance cases; 2 for net reduced clearance cases @ T = 204 and 315 °C; 3 for net reduced clearance cases @ T = 426 °C.

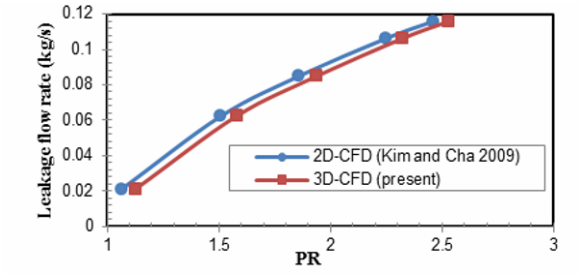

(a)

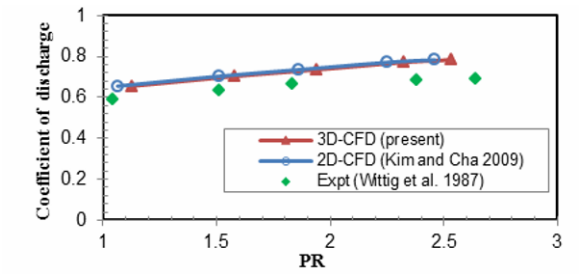

(b)

Fig. 4. Validation for CFD model: (a) variation of leakage flow rate with PR; (b) variation of coefficient of discharge with PR.

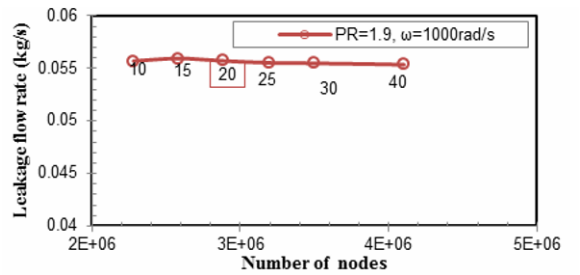

Fig. 5. Grid independence study (CFD) for R75 with initial clearance.

maximum Mach number for the cases investigated is found to be in the range of 0.17 to 0.78. A significant variation in density and temperature across the seal are noticed owing to the compressibility effects. Thus, there is a considerable drop in density noticed for all the cases investigated. Typically, the

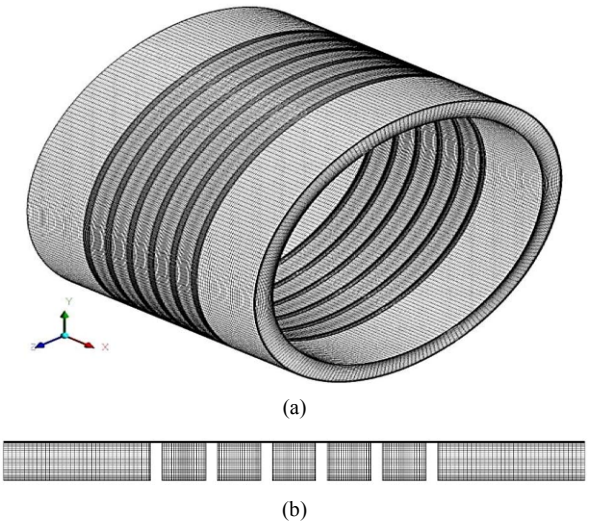

(a)

(b)

Fig. 6. CFD grid for R75: (a) 3D view; (b) upper half; along mid XY-plane.

density varies along the length of seal with a factor of up to 1.1 at PR = 1.1; and up to 2.53 at PR = 2.5 almost for all the cases investigated. Further, a significant temperature change is noticed across the seal; and the temperature change varies with the configuration and the operating conditions. For instance, the temperature varies with a factor of 1.08 across the seal for R50 configuration operating at PR = 2.5, ω = 3000 rad/s; and T = 204℃. The interesting flow features and further extension to the estimation of rotordynamic coefficients will be considered in our future work.

2.2 FE model

A detailed finite element analysis is carried out to predict the centrifugal and thermal growths of the seal for a wide range of rotational speeds and temperatures at selected locations. In practice, constant thickness strips of material are inserted into the rotating disk/shaft (in the case of turbines) to form the labyrinth teeth. Thus, the rotor which comprises of (i) the solid shaft/disk and (ii) the labyrinth seal is modeled collectively as a rotating flat disk. The radial deformation due to rotation and temperature are considered individually. As the full 3D model is computationally demanding, a 45°, 3D sector model of the rotor has been created in ANSYS Mechanical 14.

For the prediction of centrifugal growth, the linear and isotropic assumptions are made for the material. The stiffness of the material is defined in terms of Young's modulus. Density and Poisson's ratio values are provided. Inconel 718 (Ni-based super alloy) is used as the rotor material and its properties at a temperature of 21°C are furnished in Table 3. Rotation is defined along the X-axis with the angular speeds of 1000, 2000 and 3000 rad/s. This is basically an inertia load that has been applied for the entire rotor model. For representing fix-free edge condition, both axial and torsional constraints are imposed for the centre-line nodes, so as to avoid axial movement

Table 3. Rotor material properties: Inconel 718.

Property	Value
Modulus of elasticity E	199.95 GPa
Poisson's ratio v	0.294
Density ρ	8220.93 Kg/m^3
Reference temperature T_{ref}	21°C

Table 4. Temperature dependent properties of rotor: Inconel 718.

T_s (°C)	E (GPa)	v	$\alpha * 10^{-6}$ (1/°C)
204	190.30	0.280	13.55
315	184.09	0.272	13.93
426	177.88	0.271	14.35

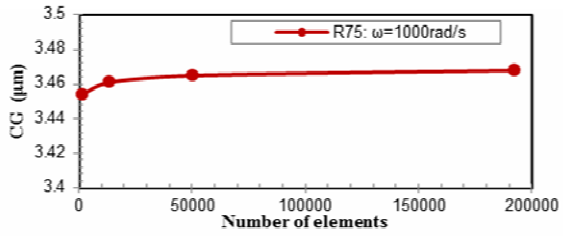

Fig. 7. Grid independence study (FEA) for R75.

and twisting. In addition, translations along the nodal Y and Z directions are suppressed for the end nodes along the centre-line, to mimic the bearing effect. Symmetry conditions are imposed on the end faces of the sector. The mass matrix formulation and a sparse direct solver are chosen.

Thermal modeling of the rotor is a difficult task owing to (i) the existence of different temperatures on the upstream and downstream surfaces of the rotor and (ii) the uncertainty in specifying the heat generation rate. For simplification, it is assumed that the temperature throughout the thickness of the rotor surface is constant and equal to the fluid temperature. Further, it is assumed that heat is neither generated nor transferred. Thus, for the thermal growth prediction, a uniform fluid temperature value is applied for the entire rotor model. The temperature dependent properties of Inconel 718 [25] for the corresponding surface temperature of the rotor are incorporated into the FE model, as furnished in Table 4. A comprehensive element insensitivity analysis [22] is carried out using SOLID 185 and SOLID 186 elements [26], which are eight and sixteen-node three dimensional structural elements. Both the elements have three translational degrees of freedom along the nodal X, Y, and Z directions. In addition, rotations along the nodal X, Y, and Z directions are added. Based on the results of insensitivity analysis, SOLID185 is chosen for the present analysis. A detailed grid independency analysis is carried out. Typical results for R75 configuration at an angular speed of 1000 rad/s is shown in Fig. 7. Fig. 8 shows the FE mesh for R75 configuration, with 13284 elements. The accuracy of sector model is ensured by comparing it with the full 360° model.

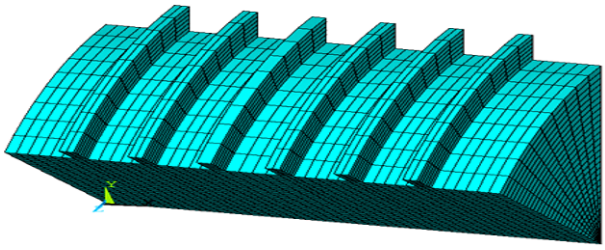

Fig. 8. 3D FE mesh for R75.

The FE results from the analysis are compared with the analytical results obtained from the rotating flat disk formulation of Timoshenko [27, 28]. The radial deformations due to rotational load and thermal load (considering the seal mounted on a solid shaft) can be expressed using Eqs. (1) and (2).

$$U_{CG} = \frac{\rho\omega^2 r^3(1-\nu)}{4E} \tag{1}$$

where $\omega = \frac{2\pi N}{60}$

$$U_{TG} = \alpha r(T_s - T_{ref}). \tag{2}$$

The comparison between the FEA and analytical results are discussed in Sec. 3.2.

3. Results and discussion

Three different angular velocities ranging from 1000 to 3000 rad/s, six pressure ratios in the range of 1.1 to 2.5, three different locations (R25, R50 and R75) are chosen, to study their effects on the leakage performance.

3.1 Location influences on leakage performance for initial clearance

Fig. 9 depicts the leakage performance characteristics as a function of rotational speed and pressure ratio for an initial clearance 0.5 mm at different locations. The trend agrees closer to the earlier works reported in Zhigang Li et al. [16] for staggered labyrinth seal; and Andres and Ashton [29] for different class of rotating seals. The influence of rotational speed and pressure ratio on leakage at different locations of interest is quantified in terms of percentage reduction in leakage flow rate (PRLF) with respect to the static case. Fig. 10 shows the variation of PRLF with PR at different locations for varying speeds. In general, the leakage flow rate increases with pressure ratio and decreases with rotational speed. However, rotation has varying influence on leakage at different locations. It is more prominent at low pressure ratios at all locations and steadily increases as the pressure ratio is increased, from a value close to zero (for small rotor) to about 25% for a large rotor. Thus, the percentage reduction decreases with increasing pressure ratio and increases with rotational speed for almost all the cases. It is apparent from Fig. 10 that the rotation effect is more pronounced from low to mid pressure ratio (1.1 to 1.5) than from mid to high pressure ratio range regardless of the seal location. Besides, the percentage reduction in leakage flow rate increases, as the radial position of the seal increases. That is, rotation has more prominent effect for R75.

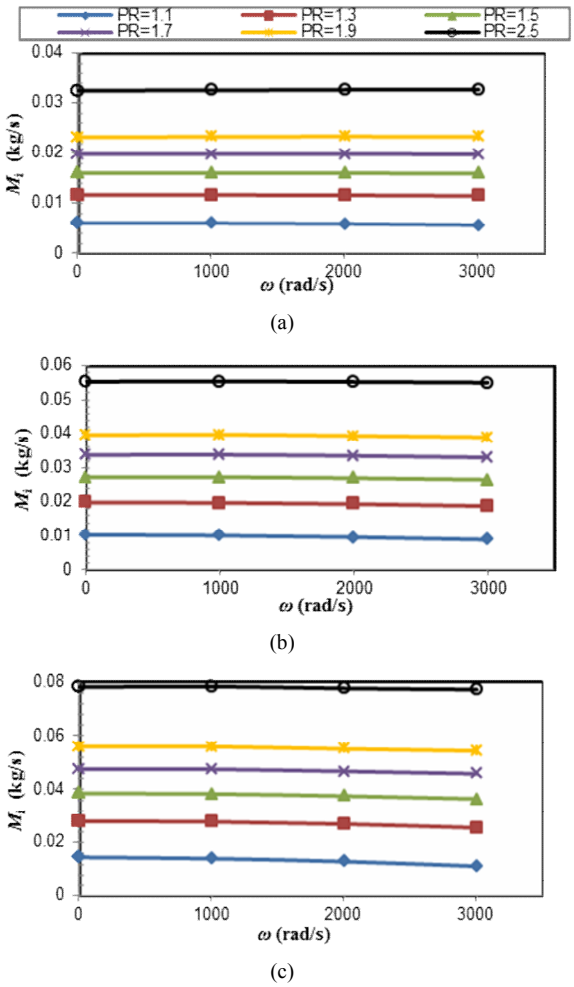

Fig. 9. Leakage flow performance at different location for initial clearance: Leakage flow rate vs. angular speed for (a) R25; (b) R50; (c) R75.

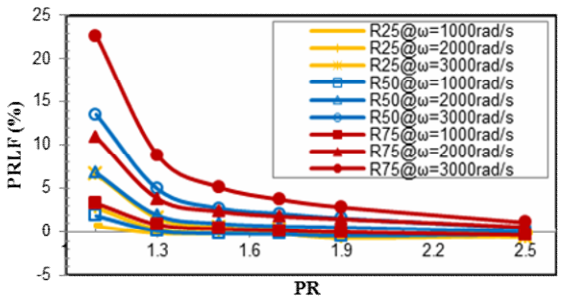

Fig. 10. Variation of PRLF with PR at different locations for varying speeds.

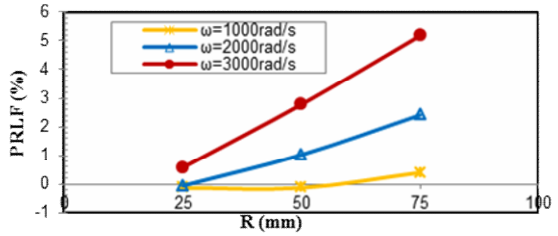

(a) PRLF vs. R @ PR = 1.5

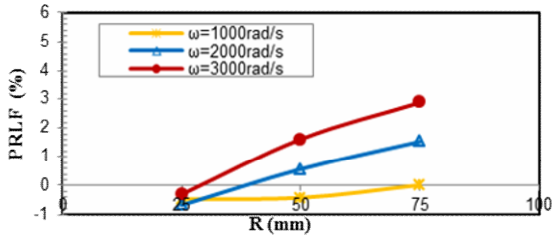

(b) PRLF vs. R @ PR = 1.9

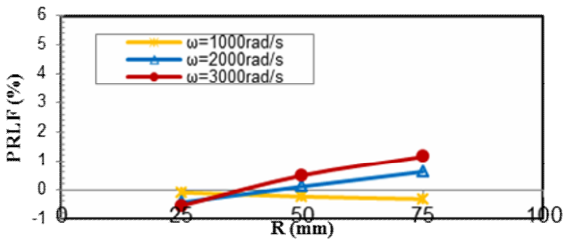

(c) PRLF vs. R @ PR = 2.5

Fig. 11. Variation of PRLF with R at a specified PR for varying speeds.

For instance, the percentage reduction corresponding to a rotational speed of 3000 rad/s and pressure ratio of 1.1 is about 7%, 14%, and 23%, respectively for R25, R50 and R75. The foregoing example illustrates that the rotation has more influence on leakage rates when the seal is located farther from the shaft axis. Fig. 11 shows the variation of percentage reduction with location at a specified pressure ratio for varying speeds and it is shown essentially to highlight the noticeable difference in trend. Typically, at low speeds and for pressure ratios of 1.5 and above, PRLF is negative or close to zero, especially for the seals placed closer to the shaft axis. The reason for this behavior could be that (i) the viscous effect is predominant than the centrifugal effect and (ii) the increased circumferential velocity leads to a reduced viscous effect, accompanied by the complex turbulent flow.

3.2 Location influences on radial growth

The comparison between FE and analytical based radial growth at the preferred locations for a wide range of rotational speed and temperature is shown in Fig. 12. Similar trend has been reported for centrifugal growth of rotor (Shaft) in Refs. [17, 18] for PDS, based on Roark's formula and FEA, respectively. Further, the trend shown in Fig. 12 for both the centrifugal and thermal growth is in line with the earlier predictions [22] for R50 configuration with fix-free end conditions. That is, the radial growth varies quadratic with rotational speed and almost linearly with temperature. Besides the trend, it is quite obvious that both the centrifugal and thermal growth increase drastically as the radial position of seal is increased for any given operating condition. The radial growth is predominant especially at elevated operating conditions for large rotor. It is observed that the analytical model over-predicts centrifugal growth by 35, 27 and 22%, respectively for R25, R50 and R75; and under-predicts thermal growth by 28, 4 and 1%, irrespective of angular speeds and temperature conditions. Nevertheless, the robustness of the analytical model can be examined by comparisons with FEA results reported in Ref. [19] for centrifugal growth prediction for similar boundary conditions. One of the labyrinth brush seals investigated by Li et al. [19] has a shaft radius of 335.5 mm, outer seal radius of 340 mm, and clearance of 0.2 mm, operating at an angular speed of 3000 rpm. The rotating flat disk model predicts the centrifugal growth as 26.21 μm (Estimated using Eq. (1)), which is reasonably closer to FEA results (25 μm), predicted by them [19]. It may be noteworthy that unlike 3D FE model, the analytical model doesn't account for the seal axial dimension details; and also the temperature dependent material properties of the rotor. Thus, the FEA based radial growth predictions can be taken as more accurate and reliable one and it has been utilized in the present investigations. Yet, the analytical model has to be assessed for a wide range of rotor sizes and class of rotating seals for its applicability, which needs extensive studies and presently is under investigation. Figs. 13 and 14 shows the typical net deformation and the true radial

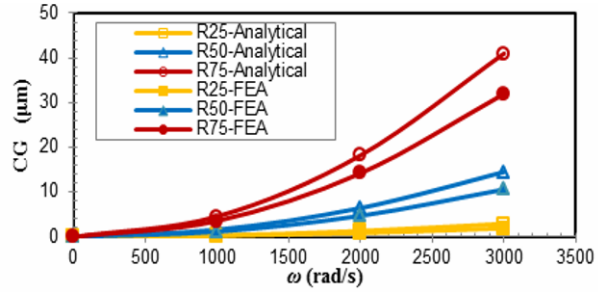

(a) Centrifugal growth vs. speed

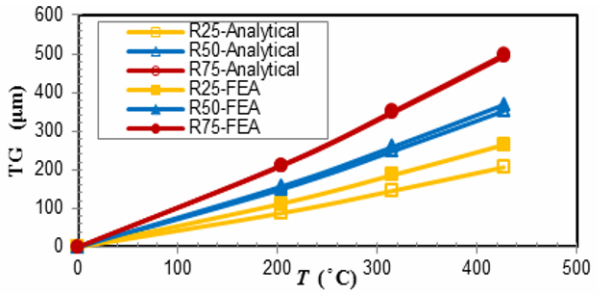

(b) Thermal growth vs. temperature

Fig. 12. Radial growth as a function of (a) angular speed; (b) temperature at different locations.

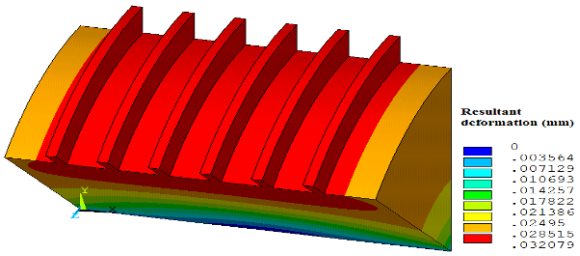

Fig. 13. Resultant deformation @ ω = 3000 rad/s for R75.

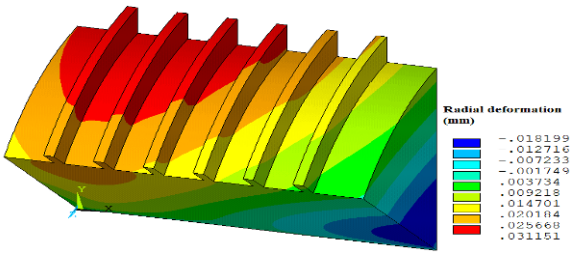

Fig. 14. True radial deformation (*CG*) @ ω = 3000 rad/s for R75.

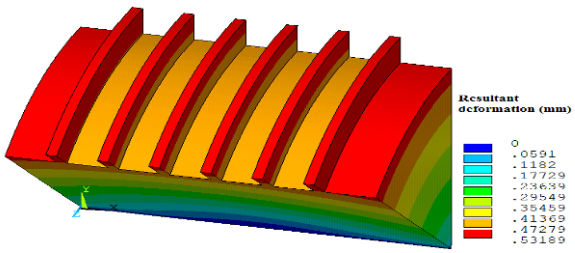

Fig. 15. Resultant deformation @ T = 426°C for R75.

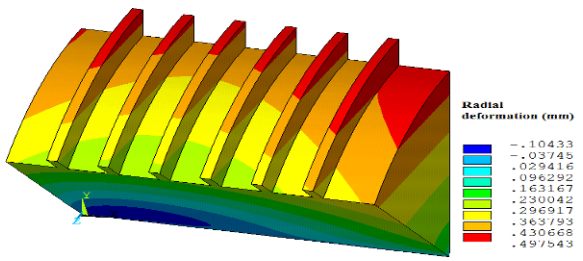

Fig. 16. True radial deformation (*TG*) @ T = 426°C for R75.

deformation (Centrifugal growth) contours respectively obtained at an angular velocity of 3000 rad/s for R75. Figs. 15 and 16 depicts the typical resultant (Total) deformation and the true radial deformation (Thermal growth) contours respectively obtained at a temperature of 426°C for R75. It is obvious that the magnitudes of the maximum true radial deformation values are lower than that of the corresponding net deformation. To avoid rubbing and to have a better sealing (Leakage) performance, the initial clearance can be decided carefully based on the maximum radial deformation values. Thus, the maximum radial deformation values are considered as the centrifugal/thermal growth of the seal and the same was utilized for determining the operating clearances.

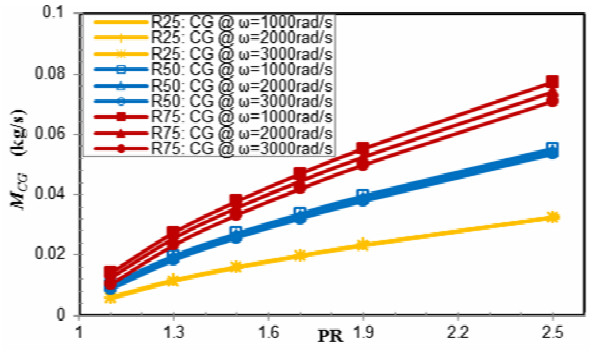

Fig. 17. Leakage flow characteristics at different locations for various angular speeds incorporating CG.

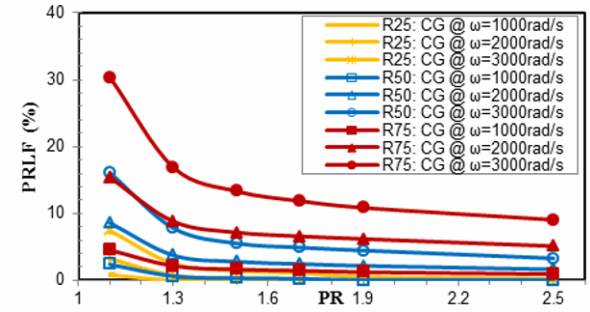

Fig. 18. Influence of CG on leakage as function of pressure ratio and angular speed at different locations.

3.3 Location influences on leakage performance considering CG alone

The CFD model is updated with the reduced operating clearance, incorporating the corresponding centrifugal growth and the leakage flow analysis has been carried out again with the reduced operating clearance for three rotational speeds: 1000, 2000, 3000 rad/s at different locations. Fig. 17 depicts the leakage flow rate at different speeds after incorporating the corresponding centrifugal growth at different locations. Similar trend has been reported in Ref. [18] for PDS.

The rotation has significant effect with the inclusion of centrifugal growth, which can be noticed particularly for higher radial position of seal. The percentage reduction in leakage flow rate is obtained using Eq. (3).

$$PRLF = \frac{M_i - M_{CG}}{M_i} \times 100 \tag{3}$$

where M_i represent leakage flow rate for static cold condition (without any growth) and M_{CG} represent leakage flow rate, for the reduced operating clearance (Considering CG alone) at a given angular speed. Fig. 18 shows the influence of centrifugal growth on leakage as a function of rotational speed and pressure ratio at different location. It is found out that the percentage reduction increases with speed and decreases slightly with pressure ratio, irrespective of location. Besides, the percentage reduction increases further with the radial position of the seal. Thus, the seal operating at high speed and placed

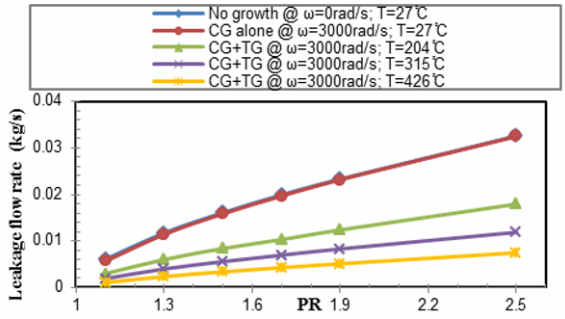

(a) Leakage flow rate vs. PR for R25

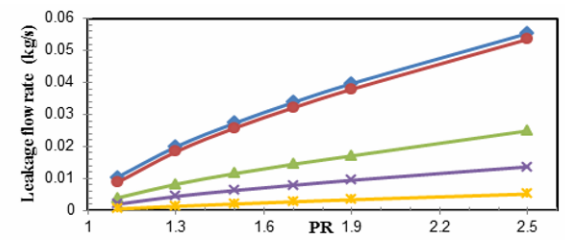

(b) Leakage flow rate vs. PR for R50

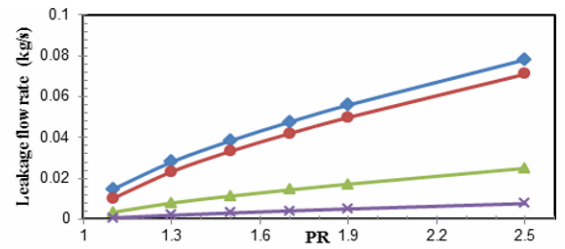

(c) Leakage flow rate vs. PR for R75

Fig. 19. Leakage flow characteristics at different locations for various temperatures incorporating both CG and TG at ω = 3000 rad/s relative to baseline.

farther from the shaft axis, experiences pronounced centrifugal growth, which results in more impact on leakage performance. The influence is more significant at low pressure high speed combinations as the centrifugal force is more dominant than the pressure force.

3.4 Location influences on leakage performance considering both CG and TG

The CFD model is updated with the net reduced operating clearance (Incorporating both CG and TG) and the leakage flow analysis has been carried out once again for a particular rotational speed of 3000 rad/s for 3 temperature conditions: 204, 315, 426°C at different locations. The density and viscosity of air at standard atmospheric pressure for the corresponding temperature conditions [30] are furnished in Table 5. Adequate care has been taken to ensure the new CFD grids generated are ascertained to have the greater level of accuracy and reliability as done earlier. Fig. 19 shows the leakage flow characteristics at a particular rotational speed 3000 rad/s, incorporating both CG and TG compared to the case of static-cold condition for various temperature conditions at different locations. The choice of operating temperature and rotational speed range depends on location; hence adequate care is given to avoid a potential rub, which may occur beyond a particular limit for a specific initial clearance. To facilitate comparison, the rotational speed has been chosen as 3000 rad/s, as lower speeds have least impact on leakage flow rate (See Fig. 18). To ensure a safe operating clearance (Say ~0.1 mm) for the chosen speed, the temperature range can be limited to 315°C and 426°C respectively for R75 and R50 configurations; and possibly little beyond 426°C for R25.

Table 5. Properties of air.

Air temperature (°C)	Density (Kg/m^3)	Viscosity *10^{-6}(Kg/m-s)
27	1.225	1.7894
204	0.7403	2.5849
315	0.601	2.972
426	0.51	3.332

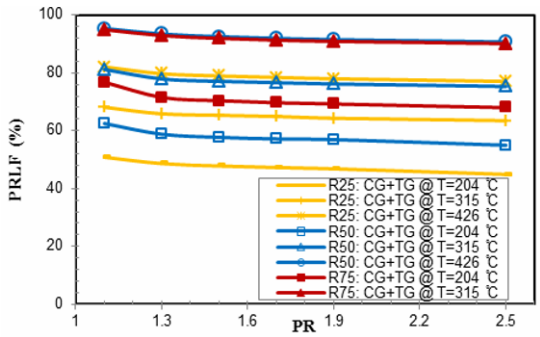

Fig. 20. Influence of combined CG and TG on leakage at ω = 3000 rad/s, as function of temperature and pressure ratio at different locations.

From Fig. 19, it is evident that the leakage flow rate decreases considerably with centrifugal growth and further gets reduced drastically as the thermal growth is also included, regardless of location. The effect is more pronounced at high temperature and high pressure ratio, as the radial position of the seal is increased. Fig. 20 shows the influence of combined radial growth on leakage as function of temperature and pressure ratio for a particular rotational speed of 3000 rad/s at different locations. The percentage reduction in leakage flow rate after incorporating both centrifugal and thermal growth is calculated using Eq. (4).

$$PRLF = \frac{M_i - M_{CTG}}{M_i} \times 100 \tag{4}$$

where M_i represent leakage flow rate for static cold condition (without any growth) and M_{CTG} represent leakage flow rate for the net reduced clearance (Considering both CG and TG) at an angular speed of 3000 rad/s. In general, as seen from Fig. 20, higher the temperature, the greater is the reduction in leakage flow rate as reported in Ref. [29]. Besides, the percentage reduction increases with increasing radial position of the seal. Thus, the farther most seal experiences more pronounced net

growth, which eventually results in more impact on leakage performance. Moreover, it is interesting to note that there is a slight drop in percentage reduction with increasing pressure ratio while, the percentage reduction increases with temperature in a particular proportion for almost all the cases. It may be noted that the pressure ratio has less influence on the reduction in leakage flow rate, irrespective of temperature and location.

4. Conclusions

The combined influences of radial location and growth on the leakage flow performance of a six-tooth straight-through rotating labyrinth GT seal have been investigated computationally for a wide-ranging operating conditions. The combined CFD/FEA methodology adopted is validated against the available data in the open literature. The key outcomes are summarized as follows:

(1) The percentage reduction in leakage flow rate (PRLF) through the seal increases with increasing rotational speed. This effect is more prominent at pressure ratios below 1.5. The value of PRLF increases with increasing radial location of the seal. This is true for the seals with or without considering radial growth.

(2) When radial growth is not considered, typical value of PRLF is less than 1% for R25 configuration at a pressure ratio of 1.1 and a speed of 1000 rad/s. The PRLF is as high as 23% for R75 configuration at 3000 rad/s at the same pressure ratio of 1.1. Thus, the seals operating at higher pressure ratio and lower radial location are prone to higher leakages, regardless of rotational speed.

(3) At a given radial location, the centrifugal growth increases in a quadratic fashion with increasing speed. The seals located at smaller radial position show smaller centrifugal growth than those located at higher radial position. Typically, R25 configuration has a centrifugal growth of about 2 μm at 3000 rad/s. In contrast, the R75 grows by 32 μm at the same speed.

(4) The thermal growth is much larger than the centrifugal growth for the chosen operating conditions. Typically, for a temperature of 426°C, thermal growth is 264 μm for the R25 configuration and it is as high as 492 μm for the R75 configuration. The initial clearance can therefore be decided based on the operating temperature relative to cold condition.

(5) In a realistic situation, where radial growth occurs due to both centrifugal and thermal effects, the PRLF ranges from 47 to 82% for R25 configuration, whereas the range is between 69 and 95% for R75 configuration for the chosen operating conditions of interest.

(6) The three-dimensional FE model developed has shown the shortcomings in the analytical model for determining the radial growth accurately, thereby stressing the need for a detailed assessment of analytical model for a wide range of rotor sizes for different class of rotating GT seals, which is under investigation.

From the present findings, it is obvious that a prior understanding of combined location and radial growth influences in detail may enable the GT engineers to decide about an initial clearance judiciously, which aids in designing secondary air systems more reliable and efficient. It could be noted that in a real engine or component test, the stator also experiences thermal growth, which needs to be accounted for predicting the actual leakage flow rate.

Acknowledgment

The authors express their profound gratitude to the Centre for Computational Fluid Dynamics and High Performance Computing Facility, IIT Madras; and Gas Turbine Research Establishment (GTRE), Bengaluru for the generous support. The authors are also grateful to Prof. E. G. Tulapurkara, Department of Aerospace Engineering, IIT Madras for his valuable time and comments on the manuscript.

Nomenclature

b	: Width of the seal tooth
C	: Initial (static cold) clearance
C_1	: Reduced operating clearance due to CG alone
C_2	: Net reduced operating clearance due to combined CG &TG
CG	: Centrifugal growth of seal
E	: Modulus of elasticity of the rotor material
h	: Height of the seal tooth
L	: Length of the shaft
M_i	: Leakage flow rate for initial clearance
M_{CG}	: Leakage flow rate for reduced operational clearance
M_{CTG}	: Leakage flow rate for net reduced operational clearance
n	: Number of teeth
p	: Pitch of the seal tooth
PR	: Pressure ratio
$PRLF$	: Percentage reduction in leakage flow rate
R	: Radius of the shaft/disk (also inner radius of seal)
r	: Tip radius of rotor (also outer radius of seal); r = R + h
TG	: Thermal growth of seal
T_s	: Surface temperature of rotor
T_{ref}	: Reference temperature of rotor
U_{CG}	: Radial deformation due to CG
U_{TG}	: Radial deformation due to TG
α	: Thermal expansion coefficient for rotor material
ν	: Poisson's ratio of the rotor material
ρ	: Density of the rotor material
ω	: Angular speed of the rotor (rad/s)

References

[1] H. J. Sneck, Labyrinth seal literature survey, *Journal of Lubrication Technology*, 96 (4) (1974) 579-581.

[2] M. Hwang, A. N. Pope and B. Shucktis, Advanced seals for engine secondary flow path, *AIAA Journal of Propulsion and Power,* 12 (4) (1996) 794-799.

[3] R. E. Chupp, R. C. Hendricks and S. B. Lattime, Sealing in turbomachinery, *AIAA Journal of Propulsion and Power,* 22

(2) (2006) 313-349.

[4] J. W. Chew and N. J. Hills, Computational fluid dynamics for turbomachinery internal air systems, *Philosophical transactions of the royal society A: Mathematical, physical and engineering sciences,* 365 (1859) (2007) 2587-2611.

[5] F. E. Aslan-zada, V. A. Mammado and F. Dohnal, Brush seals and labyrinth seals in gas turbine applications, *Proceedings of the institution of mechanical engineers, Part A: Journal of Power and Energy,* 227 (2) (2013) 216-230.

[6] S. Wittig, U. Schelling, S. Kim and K. Jacobsen, Numerical predictions and measurements of discharge coefficients in labyrinth seals, *ASME, International Gas Turbine Conference and Exhibition, Anaheim, CA. ASME paper GT1987-188* (1987).

[7] D. W. Childs and J. M. Vance, Annular gas seals and rotordynamics of compressors and turbines, *Proceedings of 26th Turbomachinery Symposium,* Texas, USA (1997) 201-220.

[8] B. V. S. S. S. Prasad, V. Sethumanavalan and N. Nanjundarao, Computational and experimental investigations of straight-through labyrinth seals, *ASME Paper GT1997-326* (1997).

[9] B. V. S. S. S. Prasad, V. Sethumanavalan and N. Nanjundarao, Analysis of leakage flow through inclined labyrinth seals, *The Seventh Asian Congress of Fluid Mechanics,* Allied Publishers (1997).

[10] N. Nanjundarao, V. Sethumanavalan, B. V. S. S. S. Prasad and O. Hanumakumar, Computational and experimental investigations of leakage flow through radial labyrinth seals, *9th ISROMAC,* Hawaii, USA (2002) DD-ABS-072.

[11] T. S. Kim and K. S. Cha, Comparative analysis of the influence of labyrinth seal configuration on leakage behavior, *Journal of Mechanical Science and Technology*, 23 (10) (2009) 2830-2838.

[12] M. P. Proctor and I. R. Delgado, Leakage and power loss test results for competing turbine engine seals, *ASME paper GT2004-53935* (2004).

[13] I. R. Delgado and M. P. Proctor, Continued investigation of leakage and power loss test results for competing turbine engine seals, *Paper No. NASA / TM-2006-214420* (2006).

[14] R. Paolillo, C.-Z. Wang, T. K. Vashist, D. Cloud, F. M. G. Bingen and G. A. Kool, Rotating seal rig experiments: test results and analysis modeling, *Proceedings of ASME Turbo Expo 2006: Power for Land, Sea, and Air* (2006) 1551-1559.

[15] R. Paolillo, S. Moore, D. Cloud and J. A. Glahn, Impact of rotational speed on the discharge characteristic of stepped labyrinth seals, *Proceedings of ASME Turbo Expo 2007: Power for Land, Sea, and Air* (2007) 1291-1298.

[16] Z. Li, J. Li, X. Yan and Z. Feng, Effects of pressure ratio and rotational speed on leakage flow and cavity pressure in the staggered labyrinth seal, *ASME Journal of Engineering for Gas Turbines and Power,* 133 (11) (2011) 114503.

[17] A. M. Gamal, B. H. Ertas and J. M. Vance, High-pressure pocket damper seals: leakage rates and cavity pressures, *ASME Journal of Turbomachinery,* 129 (4) (2007) 826-834.

[18] Z. Li, J. Li, X. Yan and Z. Feng, Numerical investigations on the leakage flow characteristics of pocket damper labyrinth seals, *Proceedings of the Institution of Mechanical Engineers, Part A: Journal of Power and Energy,* 226 (7) (2012) 932-948.

[19] J. Li, B. Qiu and Z. Feng, Experimental and numerical investigations on the leakage flow characteristics of the labyrinth brush seal, *ASME Journal of Engineering for Gas Turbines and Power,* 134 (10) (2012) 102509.

[20] D. Amirante, N. J. Hills and C. J. Barnes, Use of dynamic meshes for transient metal temperature prediction, *ASME Paper GT2012-68782*.

[21] V. Ganine, U. Javiya, N. Hills and J. Chew, Coupled fluid-structure transient thermal analysis of a gas turbine internal air system with multiple cavities, *ASME Journal of Engineering for Gas Turbines and Power,* 134 (10) (2012) 102508.

[22] S. Subramanian, A. S. Sekhar and B. V. S. S. S. Prasad, Performance analysis of a rotating labyrinth seal with radial growth, *ASME Turbo Expo 2013, ASME Paper GT2013-95708,* San Antonio, USA (2013).

[23] S. Subramanian, A. S. Sekhar and B. V. S. S. S. Prasad, Influence of location on leakage performance of a rotating labyrinth gas turbine seal with radial growth, 15th *ISROMAC, Paper No. 2014-232,* Hawaii, USA (2014).

[24] T. Hirano, Z. Guo and R. G. Kirk , Application of computational fluid dynamics analysis for rotating machinery-part ii: labyrinth seal analysis, *ASME Journal of Engineering for Gas Turbines and Power,* 127 (4) (2005) 820-826.

[25] INCONEL 718 properties, *www.specialmetals.com/documents/Inconel alloy 718.pdf*.

[26] ANSYS Mechanical 14, Element description, *ANSYS Users Guide* (2011).

[27] S. P. Timoshenko and J. Goodier, *Theory of elasticity,* McGraw-Hill Book Company, New York, USA (1997).

[28] K. M. Melcher and J. A. Kypuros, Toward a fast-response active turbine tip clearance control, *Proceedings of the International Symposium on Air Breathing Engines ISABE 2003-1102* (2003).

[29] L. S. Andres and Z. Ashton, Comparison of leakage performance in three types of gas annular seals operating at a high temperature (300°c), *Tribology Transactions,* 53 (3) (2010) 463-471.

[30] Air properties, *http://www.engineeringtoolbox.com*.

A. S. Sekhar is currently a Professor of Mechanical Engineering and Head of Machine Design Section at IIT Madras. He has been awarded the Career Award for Young Teacher by the All India Council of Technical Education in1998. He did research at TU Darmstad, Germany as an Alexander von Humboldt Research Fellow in 2002. He has published over 150 papers in internationaljournals and conferences. He is the co-author of the book-*Dynamic Analysis of Rotating Systems and Applications* (Multi Science Publishing Ltd., UK). He is an editorial member of the *Journal of Advances in Mechanical Engineering* (Hindawi Publishing Corporation). His areas of research include rotor dynamics, condition monitoring and vibrations.

B. V. S. S. S. Prasad is currently a Professor and Head of Mechanical Engi- neering at IIT Madras, Chennai. He is also the principal coordinator of the CFD Centre at IIT Madras. He published more than 150 research papers in various international journals and conference proceedings. He edited 7 conference proceedings and organized several conferences and workshops. His research areas include thermo fluid dynamics related to turbomachines, energy conversion technologies and CFD. He is a life member of K-14 (Heat Transfer) group of IGTI (ASME), Fluid Mechanics and Fluid Power Society, Indian society for Heat and mass Transfer, Instrument Society of India and Fluid Power Society of India.

Sivakumar Subramanian obtained a Bachelor's degree in Mechanical Engineering from Madurai Kamaraj University, India and Master's degree from IIT Madras. Presently, he is pursuing his Doctoral studies at IIT Madras. His current research focuses on design and analysis of gas turbine seals with emphasis on leakage and rotor dynamic characteristics. His broad areas of interest include Gas turbine secondary air system, Rotor dynamics, Applied FEM/CFD, Condition monitoring and machinery diagnosis. He is a life member of Indian Society for Technical Education.